Article

Discovery Medicine 2025; 37(194): 496–502
https://doi.org/10.24976/Discov.Med.202537194.41

Machine Learning Models Based on Stretched-Exponential Diffusion Weighted Imaging to Predict TROP2 Expression in Nude Mouse Breast Cancer Models

Yi Deng[1,*], Chao-gang Han[1], Zi-qin Deng[1], Shou-yi Yang[1], Zhuo-han Wu[1], Jia-li Liu[1], Jia-ming Ma[1]

[1]Department of Radiology, Shaoguan Maternal and Child Health Hospital, 512000 Shaoguan, Guangdong, China
*Correspondence: jxdyii@126.com (Yi Deng)
Published: 20 March 2025

Background: Trophoblast cell surface antigen 2 (TROP2) is a promising target for various cancers, including breast cancer. The development of noninvasive techniques for assessing TROP2 expression in tumors holds considerable importance. This study aims to explore the efficacy of machine learning models based on multi-b-value diffusion-weighted imaging (DWI) using the stretched-exponential model (SEM) for predicting TROP2 expression in breast cancer in nude mouse models.

Materials and Methods: Thirty-two nude mouse breast cancer models were subjected to 1.5T magnetic resonance imaging (MRI). Using the freely available software package FireVoxe, we extracted the distribution diffusion coefficient (DDC) and water molecule diffusion heterogeneity index (α) values from SEM, along with histogram parameters of DDC and α maps. TROP2 expression was identified by immunohistochemical staining, with integrated optical density (IOD) quantifying the expression levels. Mice were categorized into high and low TROP2 expression groups based on the median IOD. Key imaging parameters were selected to establish three machine learning models: extreme gradient boosting (XGBoost) classifier, logistic regression, and adaptive boosting (AdaBoost) classifier. We compared the models using the area under the curve (AUC) of the receiver operating characteristic (ROC) on a validation set to determine the superior model. The dataset was split into a training set (28 cases) and a test set (4 cases). The selected model was trained to optimize its performance. We evaluated the models' predictive accuracy in estimating TROP2 expression using AUC, calibration curve, and decision curve analysis (DCA).

Results: Thirty-eight imaging parameters, including DDC, α value, and 36 histogram parameters, were extracted per sample. Using these, we identified eight key imaging parameters for constructing the machine learning models. The validation set AUC values for the XGBoost, logistic regression, and AdaBoost models were 0.828, 0.639, and 0.728, respectively, with XGBoost demonstrating superior prediction performance. In the training set, XGBoost achieved an AUC of 1, sensitivity of 0.911, specificity of 1, and accuracy of 0.954; each of these values was 1 in the test set. Cross-validation yielded an AUC of 0.689, sensitivity of 0.567, specificity of 0.567, and accuracy of 0.580. The calibration curve's Brier score was 0.044, indicating proximity to the ideal curve. DCA indicated favorable net benefits within a risk threshold range of 20–90%.

Conclusions: Machine learning models based on SEM show promise for predicting TROP2 expression in breast cancer in nude mouse models. Among the models, XGBoost demonstrated outstanding performance, suggesting its potential for clinical applications.

Keywords: stretch index model; diffusion weighted imaging; machine learning; trophoblast cell surface antigen 2; breast cancer

Introduction

Trophoblast cell surface antigen 2 (TROP2), initially identified as a transmembrane glycoprotein in invasive trophoblast cells [1], has been implicated in promoting cancer cell proliferation and migration and serving as a cell adhesion receptor [2]. TROP2 overexpression has been observed in various cancer types, including breast, gastric, and lung cancers, with high levels correlating with unfavorable prognosis [3–6]. In breast cancer, TROP2 is particularly prevalent, notably in triple-negative breast cancer (TNBC) [7], where its heightened expression correlates with poorer outcomes.

TNBC is one of the most aggressive forms of breast cancer [4,6], characterized by high relapse rates and a poor prognosis. We used MDA-MB-231 breast cancer cells, a model of TNBC, in this study. Notably, research has highlighted the efficacy of TROP2 antibodies in targeting TROP2-positive breast cancer cells [4,8], with antigen-drug conjugates (ADCs) showing promise as potential treatments for TNBC and other breast cancer subtypes [9].

Currently, the assessment of TROP2 expression in tumor tissue relies on invasive procedures such as biopsy or postoperative sampling. However, these methods are limited in their ability to capture tumor heterogeneity and are susceptible to sampling errors.

The stretched-exponential model (SEM) based on multi-b value diffusion-weighted imaging (DWI) is an advanced diffusion imaging technique to calculate the distribution diffusion coefficient (DDC) and α value, reflecting average diffusivity and diffusivity heterogeneity within voxels, respectively, which is initially introduced by Bennett *et al*. [10]. DDC can noninvasively assess the tumor cell proliferation status [11,12]. Additionally, α values and DDC have been found to differ significantly between malignant and benign breast lesions [13]. Compared with conventional diffusion parameters, the water molecular diffusion heterogeneity index provided by SEM enhances tumor grading, particularly in gliomas [14,15]. Histogram analysis, a mathematical tool widely employed in oncology research, facilitates the comprehensive evaluation of tumor biological characteristics, particularly in tumor heterogeneity [16].

In the medical field, machine learning models have gained prominence for their superiority over traditional statistical modeling approaches [17]. Our study aimed to establish various machine learning models to identify the optimal one capable of recognizing TROP2 expression states.

Materials and Methods

Establishment of Animal Models

Planting human breast cancer cells into mice to establish xenogeneic breast cancer models is a commonly used method in scientific research [18,19]. Four-week-old female BALB/c nude mice (weighing 15–20 g) were sourced from Jiangxi Zhonghong Boyuan Biotechnology Co., Ltd. (animal license number: SCXK (Su) 2023-0009). Following a period of adaptive feeding, 0.1 mL of MDA-MB-231 human breast cell suspension (CL-0150B; Pronosei) containing 1×10^7 cells was subcutaneously injected into the axilla of nude mice. Cell identification was confirmed through short tandem repeats (STR) testing, and mycoplasma testing returned negative results. Tumor growth was monitored, and upon reaching a volume of 0.2 cm^3, mice were euthanized under anesthesia with an isoflurane overdose of 5%. Tumor tissue was dissected and divided into 2 × 2 mm blocks for transplantation. For transplantation, mice were anesthetized with 3% isoflurane inhalation, and the skin of the fourth pair of mammary glands on the right was disinfected and prepared by creating a small incision measuring 0.3 cm. The mammary gland was exposed and separated with tweezers, and the tumor block was inserted. The incision was sutured, disinfected, and the mouse was kept warm until recovery. Tumor formation occurred between 18 and 37 days after xenografting, with tumors reaching a maximum diameter of 5–12 mm. Mice were housed under controlled conditions, with temperature maintained at 20–26 °C, humidity at 40%–70%, and provided ad libitum access to food and water. A total of 32 breast cancer mouse models were generated.

Magnetic Resonance Imaging (MRI) Acquisition

Breast MR scans of nude mice were conducted using a 1.5T MR scanner (Signa Explorer 1.5T, General Electric Healthcare, Chicago, IL, USA) equipped with a dedicated 8-channel small animal coil. The mice were anesthetized via isoflurane inhalation. Initially, deep anesthesia was induced with 3.5% isoflurane and maintained at 2.5% isoflurane throughout the procedure. Imaging was performed with the mice in the supine position within the coil. Axial multi-b value DWI parameters were applied, including single-shot fast spin-echo, echo-planar imaging, with a field of view (FOV) of 8 × 8 cm, a matrix of 128 × 128, slice thickness/gap of 2 mm/0 mm, repetition time (TR) of 6374 ms, time to echo (TE) of 133.2 ms, and diffusion sensitivity with b-values 0, 25, 50, 100, 150, 200, 400, 600, and 800 s/mm^2. Additionally, axial T2-weighted (T2WI) and T1-weighted (T1WI) imaging sequences were included in the scan.

Image Post-Processing

All images were in Digital Imaging and Communications in Medicine (DICOM) format and processed using FireVoxel software (Build 431A, Artem Mikheev and Henry Rusinek Center for Biomedical Imaging, New York University, NY, USA), available at https://firevoxel.org/. The tumor volume was manually delineated layer by layer on the B = 0 DWI image, with reference to the T2WI image, to generate a three-dimensional region of interest encompassing the entire tumor. FireVoxel software was utilized to calculate DDC and α values and, generate DDC and α maps.

The stretched-exponential diffusion equation ($S = S_0 \times \exp((-b \times DDC)^{\alpha})$) was employed, where α represents the intravoxel water molecular diffusion heterogeneity (ranging from 0 to 1), and DDC denotes the mean intravoxel diffusion rate. Three-dimensional histogram parameters of tumor DDC and α maps were analyzed using FireVoxel.

Immunohistochemical Staining

Following imaging completion, the mice were euthanized with an isoflurane overdose of 5%. Tumors were excised, and tissue sections underwent immunohistochemical staining using a TROP2 antibody (DF3080, Affinity, diluted to 1/100). TROP2 expression, observed in the cell membranes and cytoplasm, was evaluated. Diaminobenzidine (DBA)-positive cells were stained brownish-yellow, with nuclei counterstained blue. Whole TROP2 immunostained sections were initially examined under a low-power

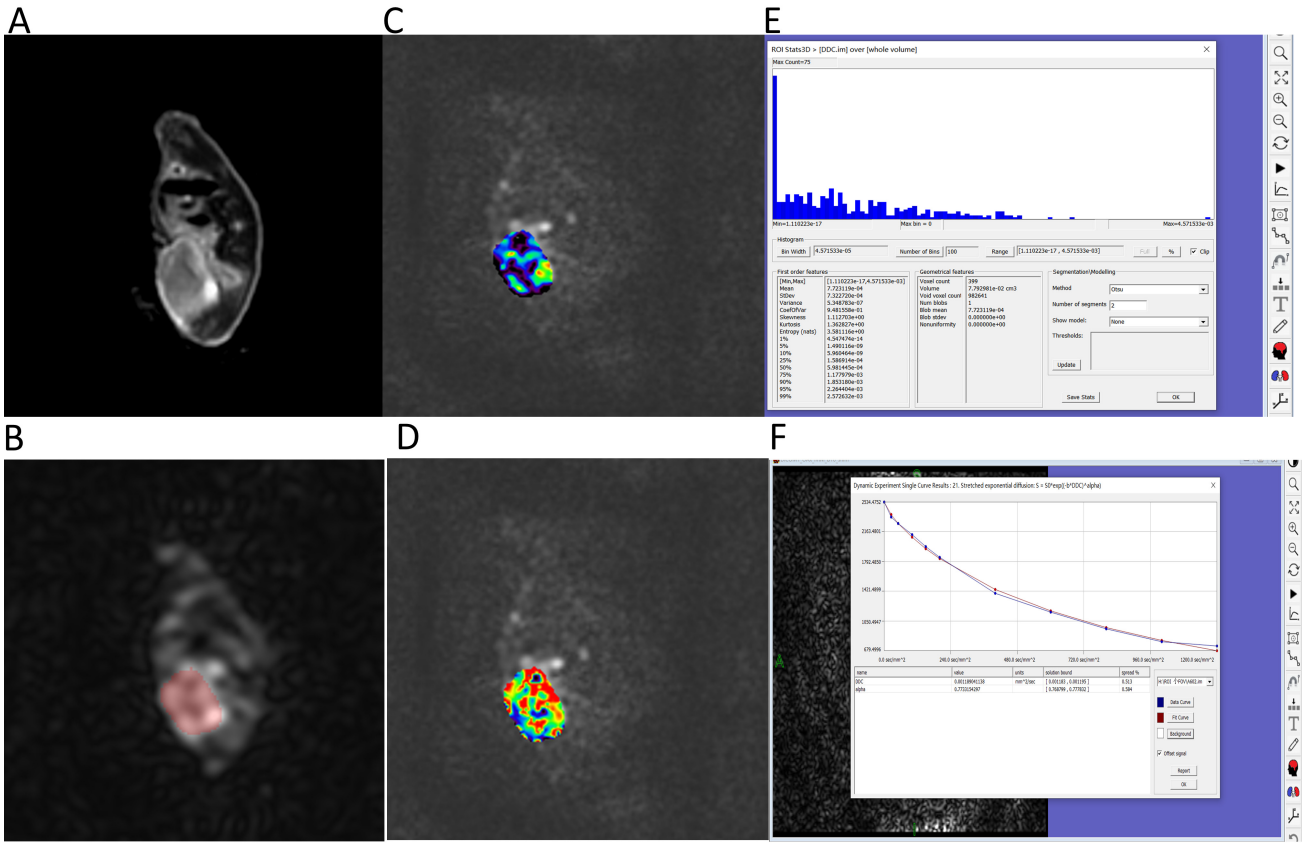

Fig. 1. The image post-processing. (A) T2-weighted imaging. (B) Diffusion-weighted imaging (DWI) with B = 0, where the highlighted pink area indicates the lesion in this slice image. (C) Distribution diffusion coefficient (DDC) map of the tumor. (D) α map of the tumor. (E) Histogram analysis of stretch index model parameters. (F) Measured DDC and α values.

microscope to identify the three areas with the densest staining, followed by high-power microscopy imaging. Image-Pro Plus 6 software (Media Cybernetics, Rockville, MD, USA) was utilized to measure the integrated optical density (IOD) across the entire image range per sample, with an average of three IODs recorded as the sample's IOD. Higher IOD values correspond to increased protein expression levels.

Machine Learning Model Exploration and Evaluation

Based on the median IOD of TROP2, the mice were categorized into high (n = 16) and low (n = 16) expression groups. Data cleansing and Z-score normalization were performed on the variable data within each group.

Extreme gradient boosting (XGBoost), logistic regression, and adaptive boosting (AdaBoost) classifiers were employed to identify the important parameters. Fifteen parameters were selected from each model, and those appearing in all three models were further explored. A multi-model comparison was conducted, and the model with the highest validation set area under the curve (AUC) of the receiver operating characteristic (ROC) was selected.

Subsequently, the selected model was refined, and a final model was developed. The dataset was divided into a training set of 28 cases and a test set of 4 cases and subjected to 10-fold cross-validation. Model performance was evaluated using receiver operating characteristic (ROC) analysis, with calibration curves employed to assess model calibration. Smaller Brier scores and calibration curves closer to the diagonal indicate better model consistency. Clinical utility was assessed using decision curve analysis (DCA).

Statistical Analysis

All statistical analyses were conducted using R (version 4.2.3, University of Auckland, Oakland, New Zealand), Python (version 3.11.4, Python Software Foundation, Amsterdam, Netherlands), and MedCalc (version 15.8, MedCalc Software Ltd, Ostend, Belgium) software.

Results

All 32 breast cancer models of the MDA-MB-231 nude mice underwent successful MRI, resulting in satisfactory image quality. The image post-processing is depicted in Fig. 1.

Each sample was analyzed for 38 parameters derived from the multi-b value DWI stretch index model, including

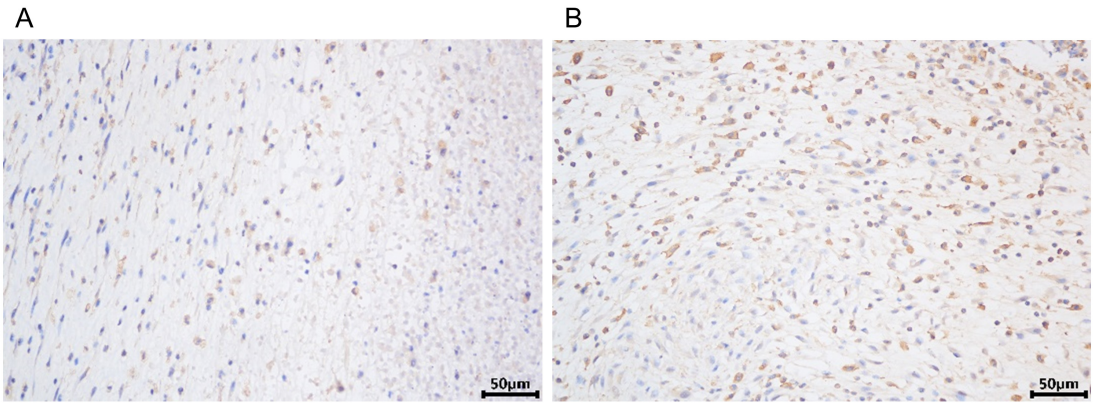

Fig. 2. Pathological images. (A) Trophoblast cell surface antigen 2 (TROP2) immunohistochemistry at magnification 400×, with an integrated optical density (IOD) of 10,148.51. (B) TROP2 immunohistochemistry at magnification 400×, with an IOD of 73,351.75.

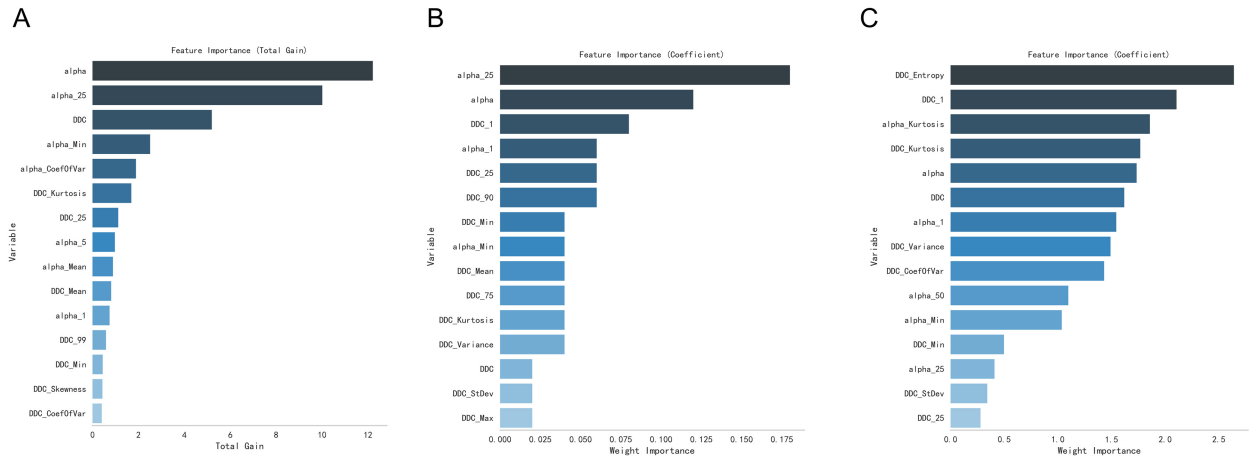

Fig. 3. Key parameters from the three methods are organized based on their respective weights. (A) Extreme gradient boosting (XGBoost) method, (B) adaptive boosting (AdaBoost) method, and (C) logistic regression.

DDC, α, min, max, mean, standard deviation (StDev), variance, coefficient of variation (CoefOfVar), skewness, kurtosis, entropy, and percentiles 1%, 5%, 10%, 25%, 50%, 75%, 90%, 95%, and 99%.

Two examples of pathological images are shown in Fig. 2.

In the low TROP2 expression group, the integrated optical density (IOD) was 30,439.27 (95% CI: 10,957.04–43,706.62), while in the high TROP2 expression group, it was 83,903.24 (95% CI: 65,668.57–116,394.09). A Mann-Whitney U test showed a statistically significant difference ($p < 0.0001$).

Immunohistochemical staining of the tumor specimens revealed a median IOD value of 5.881×10^4 for TROP2. Based on the median expression levels, the nude mice were categorized into high- and low-expression groups. The fifteen most significant parameters selected by each method are depicted in Fig. 3.

Seven parameters (alpha, alpha_1, alpha_25, alpha_Min, DDC, DDC_25, and DDC_Min) were identified as important across all three methods and used to construct the final model. Table 1 and Fig. 4 illustrate the validation set performance of the various models, with XGBoost emerging as the optimal choice for this dataset.

The final model, detailed in Table 2 and Fig. 5, demonstrates good calibration. In the training set, the XGBoost model exhibited excellent performance, with an AUC of 1, sensitivity of 0.911, specificity of 1, and accuracy of 0.954. Similarly, in the test set, the XGBoost model demonstrated an AUC of 1, sensitivity of 1, specificity of 1, and accuracy of 1. Cross-validation revealed an AUC of 0.689, sensitivity of 0.567, specificity of 0.567, and accuracy of 0.580. The DCA curves for the model surpassed the extreme assumption lines, indicating net benefits. The Brier score of the XGBoost model's calibration curve was 0.044.

Discussion

This study represents the first attempt, to our best knowledge, to predict TROP2 expression status in breast cancer using MRI. Utilizing advanced SEM techniques, we obtained DDC and α values, as well as histogram param-

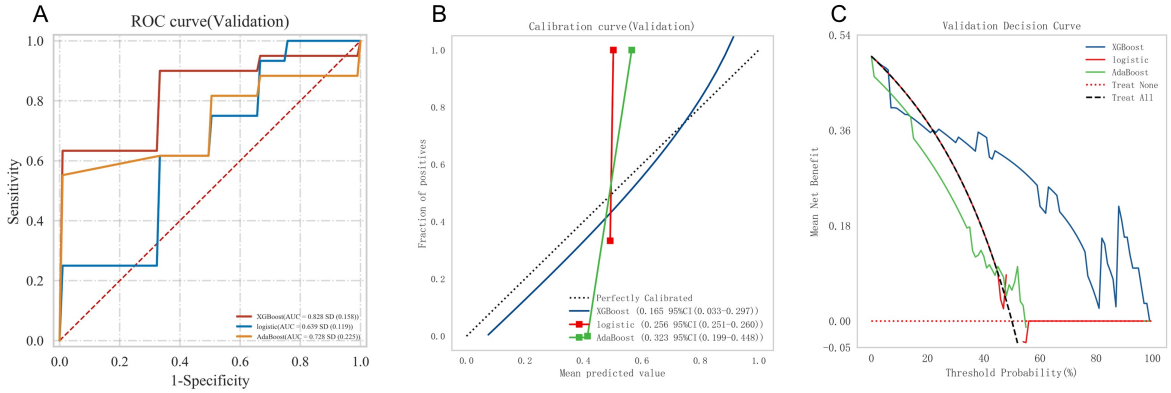

Fig. 4. Evaluation of the performance of the three models. (A) Receiver operating characteristic (ROC) curves of the models. (B) Calibration curves are used to assess model calibration. The calibration curve (blue line) of the XGBoost model closely aligns with the perfectly calibrated line. (C) Decision curve analysis (DCA) curves of the models. Compared with the DCA curves of the logistic and AdaBoost models, the DCA curve of XGBoost is further from the two extreme lines.

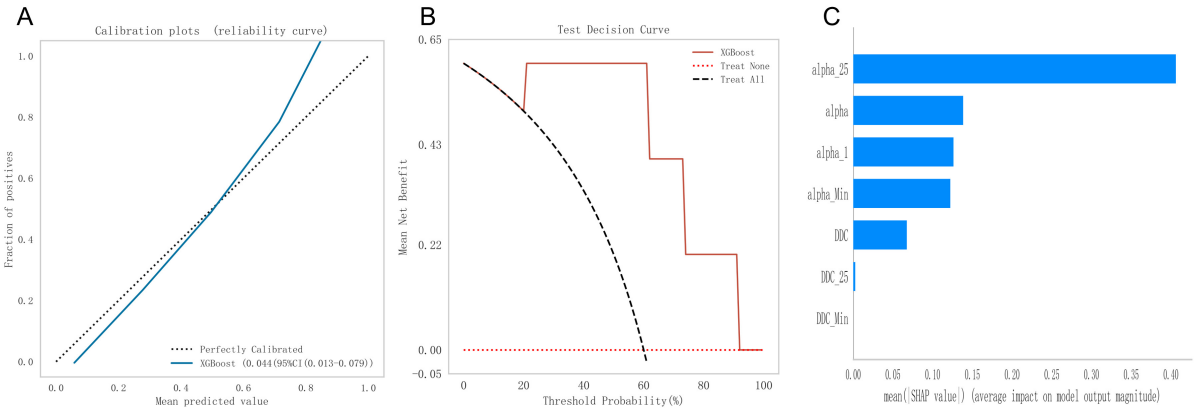

Fig. 5. Calibration curve and decision curve analysis of the model, as well as parameter ranking. (A) The calibration curve of the extreme gradient boosting (XGBoost) model, with a Brier score of 0.044. (B) Decision curve analysis (DCA) of the models. (C) The order of importance of the parameters in the model.

Table 1. Validation set performance of different models.

Models	AUC (SD)	Cutoff (SD)	Acc (SD)	Sensitivity (SD)	Specificity (SD)
XGBoost	0.828 (0.158)	0.658 (0.048)	0.690 (0.214)	0.600 (0.389)	0.817 (0.153)
Logistic	0.639 (0.119)	0.499 (0.014)	0.605 (0.180)	0.633 (0.371)	0.567 (0.133)
AdaBoost	0.728 (0.225)	0.668 (0.115)	0.624 (0.131)	0.433 (0.249)	0.833 (0.211)

AUC, area under the curve; Acc, Accuracy; CI, confidence interval.

Table 2. Prediction performance of the XGBoost model.

Data set	AUC (SD)	Cutoff (SD)	Acc (SD)	Sensitivity (SD)	Specificity (SD)
Training set	1.000 (0.000)	0.614 (0.065)	0.954 (0.001)	0.911 (0.003)	1.000 (0.000)
Cross-validation set	0.689 (0.178)	0.614 (0.065)	0.580 (0.223)	0.567 (0.249)	0.567 (0.327)
Test set	1.000 (0.000)	0.640 (0.000)	1.000 (0.000)	1.000 (0.000)	1.000 (0.000)

eters derived from DDC and α maps through histogram analysis. By employing various machine learning modeling methods, we achieved satisfactory predictive model outcomes.

In both the training and test sets, the XGBoost model exhibited excellent performance. Particularly noteworthy was the Brier score of the XGBoost model's calibration curve, which at 0.044, indicated excellent calibration per-

formance. According to previous literature, a useful forecasting tool's Brier score should not exceed 0.25 [20]. DCA showcased favorable net benefits within risk thresholds ranging from 20% to 90%.

Our findings align with those of previous studies, which also highlight the superior performance of XGBoost compared with other machine learning models [21,22]. The parameter importance ranking in the XGBoost model, based on average Shapley Additive Explanations (SHAP) values, emphasized the significant contribution of α and its histogram parameters to the model, surpassing DDC and DDC map histogram parameters.

TROP-2 promotes tumor growth, with its expression levels being directly proportional to tumor aggressiveness [2]. A study revealed a significant correlation between heightened TROP2 expression in cervical cancer tissues and the presence of Ki67-positive proliferating cells [23]. Notably, an association was observed between TROP2's effects on tumor cells and the movement of water molecules. DDC and α values represent the mean intravoxel diffusion rate and intravoxel water molecular diffusion heterogeneity, respectively. These values are typically calculated by averaging the DDC and α values of ROI voxels. Additionally, histogram analysis enhances these values by capturing the heterogeneity of these parameters within voxels more effectively.

Previous studies have showcased the effectiveness of SEM histogram analysis utilizing the entire tumor volume in predicting microvascular invasion in hepatocellular carcinoma [24] and assessing clinically significant prostate cancer [25]. Similarly, SEM histogram analysis has demonstrated promising diagnostic utility in the differential diagnosis of benign and malignant breast lesions, outperforming ADC parameters derived from a monoexponential model [26].

Our study represents an initial exploratory effort to predict TROP2 expression in breast cancer using multiparameter machine learning-based MRI. Our preliminary results are promising, and we believe this study will serve as a catalyst for more researchers to engage in this area in the future. The ultimate aim is to furnish valuable information for clinical decision-making and to alleviate the pain and costs associated with obtaining such information for patients.

However, this study is subject to several limitations. Firstly, it is a single-center study and necessitates external validation in future research. Secondly, being a preliminary animal experimental study with a small sample size, further investigation is warranted to assess its clinical applicability through larger, multicenter studies.

Conclusions

In conclusion, we have developed a machine-learning model for the noninvasive assessment of TROP2 expression in breast cancer. Our findings underscore the application value of SEM-based machine learning models in predicting TROP2 expression status in breast cancer in nude mice, with the XGBoost model demonstrating superior performance among all the machine learning models evaluated in this study.

Availability of Data and Materials

The datasets used and analyzed during the current study are available from the corresponding author upon reasonable request.

Author Contributions

YD and CH designed the research study. ZD, SY, CH and ZW performed the research. YD, JL and JM analyzed the data. All authors were involved in the drafting and critical revision of the manuscript. All authors have read and approved the final manuscript. All authors have participated sufficiently in the work and agreed to be accountable for all aspects of the work.

Ethics Approval and Consent to Participate

The study protocol underwent review and approval by the Experimental Animal Welfare and Ethics Committee of Jiangxi Zhonghong Boyuan Biotechnology Co., Ltd. (Approval No. LL-202301110005). We strictly adhered to the guidelines of the Institutional Laboratory Animal Care and Use Manual.

Acknowledgment

Not applicable.

Funding

This work was supported by the Shaoguan Science and Technology Plan Project (220520184531789).

Conflict of Interest

The authors declare no conflict of interest.

References

[1] Lipinski M, Parks DR, Rouse RV, Herzenberg LA. Human trophoblast cell-surface antigens defined by monoclonal antibodies. Proceedings of the National Academy of Sciences of the United States of America. 1981; 78: 5147–5150.

[2] Trerotola M, Cantanelli P, Guerra E, Tripaldi R, Aloisi AL, Bonasera V, *et al*. Upregulation of Trop-2 quantitatively stimulates human cancer growth. Oncogene. 2013; 32: 222–233.

[3] Zheng Z, Dong XJ. Clinical value of serum trophoblast cell surface protein 2 (TROP2) antibody in non-small-cell lung cancer patients. Biomarkers. 2016; 21: 739–742.

[4] Son S, Shin S, Rao NV, Um W, Jeon J, Ko H, *et al*. Anti-Trop2 antibody-conjugated bioreducible nanoparticles for tar-

geted triple negative breast cancer therapy. International Journal of Biological Macromolecules. 2018; 110: 406–415.

[5] Zhao W, Zhu H, Zhang S, Yong H, Wang W, Zhou Y, *et al*. Trop2 is overexpressed in gastric cancer and predicts poor prognosis. Oncotarget. 2016; 7: 6136–6145.

[6] Lin H, Huang JF, Qiu JR, Zhang HL, Tang XJ, Li H, *et al*. Significantly upregulated TACSTD2 and Cyclin D1 correlate with poor prognosis of invasive ductal breast cancer. Experimental and Molecular Pathology. 2013; 94: 73–78.

[7] Bardia A, Mayer IA, Vahdat LT, Tolaney SM, Isakoff SJ, Diamond JR, *et al*. Sacituzumab Govitecan-hziy in Refractory Metastatic Triple-Negative Breast Cancer. The New England Journal of Medicine. 2019; 380: 741–751.

[8] Wen Y, Ouyang D, Zou Q, Chen Q, Luo N, He H, *et al*. A literature review of the promising future of *TROP2*: a potential drug therapy target. Annals of Translational Medicine. 2022; 10: 1403.

[9] Stenvang J, Vestlev PM, Jensen BV, Pfeiffer P. Antibody-drug conjugates (ADCs) targeting trophoblast cell surface antigen 2 (Trop-2) and precision treatment of breast cancer. Annals of Translational Medicine. 2022; 10: 1184.

[10] Bennett KM, Schmainda KM, Bennett RT, Rowe DB, Lu H, Hyde JS. Characterization of continuously distributed cortical water diffusion rates with a stretched-exponential model. Magnetic Resonance in Medicine. 2003; 50: 727–734.

[11] Zhang G, Yan R, Liu W, Jin X, Wang X, Wang H, *et al*. Use of biexponential and stretched exponential models of intravoxel incoherent motion and dynamic contrast-enhanced magnetic resonance imaging to assess the proliferation of endometrial carcinoma. Quantitative Imaging in Medicine and Surgery. 2023; 13: 2568–2581.

[12] Chaudhary N, Zhang G, Li S, Zhu W. Monoexponential, biexponential and stretched exponential models of diffusion weighted magnetic resonance imaging in glioma in relation to histopathologic grade and Ki-67 labeling index using high B values. American Journal of Translational Research. 2021; 13: 12480–12494.

[13] Jin YN, Zhang Y, Cheng JL, Zheng DD, Hu Y. Monoexponential, Biexponential, and stretched-exponential models using diffusion-weighted imaging: A quantitative differentiation of breast lesions at 3.0T. Journal of Magnetic Resonance Imaging. 2019; 50: 1461–1467.

[14] Bai Y, Lin Y, Tian J, Shi D, Cheng J, Haacke EM, *et al*. Grading of Gliomas by Using Monoexponential, Biexponential, and Stretched Exponential Diffusion-weighted MR Imaging and Diffusion Kurtosis MR Imaging. Radiology. 2016; 278: 496–504.

[15] Sun L, Zhu W, Chen X, Jiang J, Ji Y, Liu N, *et al*. Machine Learning to Predict Contrast-Induced Acute Kidney Injury in Patients With Acute Myocardial Infarction. Frontiers in Medicine. 2020; 7: 592007.

[16] Just N. Improving tumour heterogeneity MRI assessment with histograms. British Journal of Cancer. 2014; 111: 2205–2213.

[17] Chao X, Wang S, Lang J, Leng J, Fan Q. The application of risk models based on machine learning to predict endometriosis-associated ovarian cancer in patients with endometriosis. Acta Obstetricia et Gynecologica Scandinavica. 2022; 101: 1440–1449.

[18] Cai Y, Zheng Y, Gu J, Wang S, Wang N, Yang B, *et al*. Betulinic acid chemosensitizes breast cancer by triggering ER stress-mediated apoptosis by directly targeting GRP78. Cell death & disease. 2018; 9: 636.

[19] Shetti D, Zhang B, Fan C, Mo C, Lee BH, Wei K. Low Dose of Paclitaxel Combined with XAV939 Attenuates Metastasis, Angiogenesis and Growth in Breast Cancer by Suppressing Wnt Signaling. Cells. 2019; 8: 892.

[20] Steyerberg EW, Vickers AJ, Cook NR, Gerds T, Gonen M, Obuchowski N, *et al*. Assessing the performance of prediction models: a framework for traditional and novel measures. Epidemiology. 2010; 21: 128–138.

[21] Pei X, Deng Q, Liu Z, Yan X, Sun W. Machine Learning Algorithms for Predicting Fatty Liver Disease. Annals of Nutrition & Metabolism. 2021; 77: 38–45.

[22] Chen YY, Lin CY, Yen HH, Su PY, Zeng YH, Huang SP, *et al*. Machine-Learning Algorithm for Predicting Fatty Liver Disease in a Taiwanese Population. Journal of Personalized Medicine. 2022; 12: 1026.

[23] Liu T, Liu Y, Bao X, Tian J, Liu Y, Yang X. Overexpression of TROP2 predicts poor prognosis of patients with cervical cancer and promotes the proliferation and invasion of cervical cancer cells by regulating ERK signaling pathway. PLoS ONE. 2013; 8: e75864.

[24] Li H, Wang L, Zhang J, Duan Q, Xu Y, Xue Y. Evaluation of microvascular invasion of hepatocellular carcinoma using whole-lesion histogram analysis with the stretched-exponential diffusion model. The British Journal of Radiology. 2022; 95: 20210631.

[25] Kim E, Kim CK, Kim HS, Jang DP, Kim IY, Hwang J. Histogram analysis from stretched exponential model on diffusion-weighted imaging: evaluation of clinically significant prostate cancer. The British Journal of Radiology. 2020; 93: 20190757.

[26] Liu C, Wang K, Li X, Zhang J, Ding J, Spuhler K, *et al*. Breast lesion characterization using whole-lesion histogram analysis with stretched-exponential diffusion model. Journal of Magnetic Resonance Imaging. 2018; 47: 1701–1710.